Effect of reagent translation on the dynamics of the exothermic reaction Ba+HF

Arunava Gupta, David S. Perry,[a] and Richard N. Zare

Department of Chemistry, Stanford University, Stanford, California 94305
(Received 13 November 1979; accepted 12 December 1979)

The Ba + HF(v = 0) → BaF + H reaction has been studied as a function of relative collision energy (3–13 kcal/mole) using a crossed beam geometry in which a seeded HF beam intersects a thermal Ba beam. The vibrational and rotational distributions of the BaF product are determined from computer simulations of its excitation spectrum. The reaction cross section is found to have a low threshold (~ 1 kcal/mole). With increasing collision energy the cross section increases to a maximum in the range of 6–8 kcal/mole. An upper bound of 15 Å^2 is placed on the absolute value of the reaction cross section. The fraction f' of energy appearing in translation, rotation, or vibration of the products is roughly constant over the range of collision energies studied with nearly half going into product translation and the remainder being divided nearly equally between product rotation and vibration. However, while $<f'_{rot}>$ increases slowly with collision energy, $<f'_{vib}>$ first rises then falls and $<f'_{trans}>$ first falls then rises, the crossover occuring at collision energies for which the reaction cross section reaches its maximum. The fractional energy disposal in the different product modes is qualitatively consistent with the calculations of phase space theory, but the detailed behavior cannot be matched. However, the product rotational distribution observed for each vibrational level agrees closely with the predictions of this model, which is a consequence of the kinematic constraint for the mass combination. The Ba + HF reaction as a function of collision energy shows both similarities and differences with the corresponding studies for Ba + HCl and Ba + HBr. Possible explanations for this contrasting behavior are presented.

I. INTRODUCTION

The quest for an understanding of those forces controlling the making and breaking of chemical bonds continues to motivate the study of elementary reaction dynamics.[1] We report here a crossed molecular beam experiment on the reaction

$$Ba + HF \rightarrow BaF + H , \qquad \Delta H^\circ_0 = -4.4 \text{ kcal/mole} , \qquad (1)$$
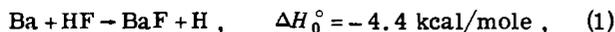
in which the internal state distribution of the BaF product is monitored by laser-induced fluorescence as a function of the reagent collision energy. Previously the Ba + HF reaction has been studied under thermal conditions[2] and with thermal HF excited to its first vibrational level, HF(v = 1).[3] In this study we explore how the state-to-state dynamics and the reaction cross section depend on reagent translational energy when HF(v = 0) is seeded in a nozzle expansion.

While molecular beam methods have been employed to determine total reaction cross sections, product translational energy, and angular distributions for a number of neutral–neutral reactions,[4] the measurement of product internal state distributions as a function of collision energy is in its infancy. In general, the latter requires a combination of spectroscopic and single collision techniques. Infrared chemiluminescence[6] and chemical laser gain[7] measurements have provided a wealth of information on the internal energy distributions of hydrogen halide products of exothermic reactions, often as a function of reagent temperature from which the role of translational energy can be inferred. More precise control of collision energy may be obtained using molecular beam techniques in which the product

state distribution is observed in visible chemiluminescence.[9–11] Here a limited range of collision energies may be obtained using thermal beams[9] or a more extended range of collision energies may be covered using nozzle expansion techniques.[10,11] We have employed the latter to vary the center of mass translational energy in the reaction Ba + HF(v = 0) over the range 3–13 kcal/mole.

We find that there is a small threshold energy for reaction. As the collision energy is increased beyond threshold, the total cross section for the Ba + HF(v = 0) reaction first rises then falls. Moreover, with increasing collision energy the product internal energy distribution spreads to higher vibrational and rotational states. The peak of the vibrational distribution first moves to higher vibrational levels and then returns to v = 0, while at the same time the total cross section passes through a maximum. We are presently unable to explain the details of the vibrational distribution, but the rotational distribution follows closely what is expected kinematically for this mass combination. Moreover, the fractional energy appearing in translation, rotation, and vibration agrees qualitatively with the predictions of phase space theory.

II. EXPERIMENTAL

A schematic diagram of the apparatus is shown in Fig. 1. The apparatus, which was described previously,[12] has been modified to study Reaction (1) under crossed beam conditions. The present arrangement allows the relative collision energy to be varied over a wide range (3–13 kcal/mole) by seeding the HF beam. The BaF products are detected by their characteristic excitation spectrum using a tunable pulsed dye laser as a probe.

[a] Present address: Department of Chemistry, University of Rochester, River Station, Rochester, New York, 14627.
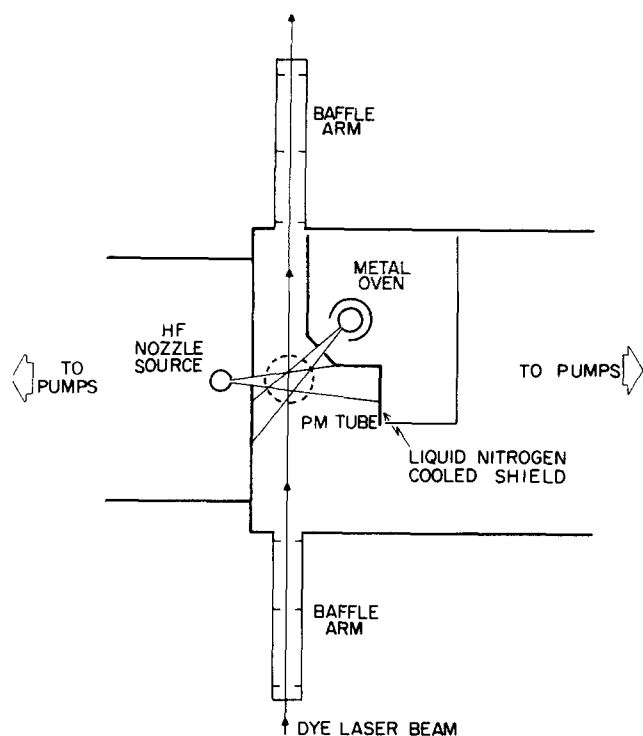
FIG. 1. Crossed molecular beam laser-induced fluorescence apparatus. The two beams intersect at 135°.

A. Crossed molecular beam apparatus

The present vacuum system has two chambers; a source chamber for the seeded HF beam, and a scattering chamber which also houses the effusive Ba source. The HF source chamber is evacuated by two 6 in. diffusion pumps and the scattering chamber by a single water-baffled 6 in. diffusion pump. A liquid-nitrogen-cooled shield in front of the barium oven cyropumps the hydrogen fluoride and it also prevents the photomultiplier tube from viewing black-body radiation from the Ba oven. The HF and Ba beams intersect at an angle of 135° rather than 90° because of the geometric constraints of the existing apparatus. The crossing region is located directly over a photomultiplier tube and is probed by a dye laser beam propagating at right angles to the HF beam.

The HF beam is formed in supersonic nozzle of diameter 0.005 in. A mixture of HF in a light carrier gas (He or H_2) is delivered to the nozzle. The HF (Matheson, 99.9%) is purified before use. The gas cylinder is placed in a dry ice acetone slush and pumped on for a few minutes to remove SiF_4 and other volatile contaminants. The hydrogen (Liquid Carbonic, 99.9%) and the helium (Liquid Carbonic, 99.995%) are used without further purification. For achieving higher translational energies, the HF source, which is a 0.375 in. monel tube, may be heated to 550 °K. The temperature of the HF source is recorded using a chromel–alumel thermocouple. The pressure of HF is held fixed while the pressure of the seeding gas is varied over the range 0 to 200 Torr. The HF beam passes through a 5×14 mm slit located 22 mm from the nozzle. The scattering center is located 5 cm from the collimating slit. The half angle of the beam divergence is thus 18°.

The Ba beam emanates from an oven placed in the scattering chamber itself. The Ba metal (Atomergic Chemmetals, 99.5%), is contained in a stainless steel crucible with a 1 mm orifice, which is surrounded by a tantalum tube. An alternating current (200–400 A) passes through this tube, indirectly heating the crucible by radiation. This assembly is surrounded in turn by a water-cooled copper jacket. The cold shield at 77 °K around the oven has a 6×18 mm slit at a distance of 4 cm from the crucible orifice. Thus, the half angle of the Ba beam is 13°. This collimating slit is 4 cm from the scattering center. The metal atom oven temperature is measured with an optical pyrometer. It should be noted that the larger dimension of both collimating slits is in the plane of the probe laser beam in order to maximize the signal intensity.

B. Detection system

The detection system is similar to what has been used previously in this laboratory.[12] A pulsed nitrogen laser (Molectron UV24) pumps a tunable dye laser (Molectron DL14P) to produce the probe beam. The BaF products are detected by exciting fluorescence in the $C^2\Pi_{1/2}$–$X^2\Sigma^+$ band system near 500 nm. For this purpose the molectron dye C500 (fluorinated coumarin) in ethanol (10^{-2}M) is used. The typical bandwidth is 0.04 nm. The pulse-to-pulse amplitude stability is better than 5% at a repetition rate of 15 Hz. The dye laser enters and exits the scattering chamber through baffle arms (0.6 m long) to minimize the scattered light. The dye laser is used without the amplifier to avoid saturation.

A photomultiplier tube (RCA 7265, 2 in. diameter, S20 photocathode), placed perpendicular to the scattering plane and to the laser beam at a distance of 6.5 cm, observes the fluorescence. A boxcar integrator (PAR model 162) averages the photomultiplier signal. The opening of the gate is almost simultaneous with the firing of the dye laser. The gate width is set at about 30 nsec, which corresponds to about twice the radiative lifetime.

C. Collision energy

Since the HF is seeded in an excess of the lighter carrier gas (H_2 or He), it is accelerated to velocities higher than those attained from a thermal effusive source.[13] In the limit of high pressures, the HF and the carrier gas approach the same velocity and the velocity distribution sharply narrows to a single value v, given by the expression

$$\int_0^{T_{\text{nozzle}}} (C_p)_{\text{mean}} \, dT = \tfrac{1}{2} M_{\text{mean}} v^2 , \tag{2}$$

where T_{nozzle} is the nozzle temperature, $(C_p)_{\text{mean}}$ is the mean molar heat capacity, and M_{mean} is the mean molecular weight of the expansion mixture.[13] In the present work it is assumed that neither HF nor H_2 experiences any rotational relaxation in the mild expansion conditions used. Neither of the gases has substantial population in vibrationally excited states at the nozzle temperatures employed. (For HF the fraction in $v=1$ at 500 °K is 7×10^{-6}). With these considerations, Eq. (2) reduces to

TABLE I. Experimental conditions and average collision energies.

Experiment	1	2	3	4	5	6	7	8
T_{HF} [a]	300	300	300	528	530	532	524	529
T_{Ba} [b]	1220	1220	1210	1220	1220	1220	1220	1220
P_{HF} [c]	32	32	32	49	49	25	25	25
P_{H_2} [d]	0	53	92	42	108	77	90	135
$\langle E_{beam} \rangle$ [e]	1.5	3.4	4.5	4.5	6.9	8.2	8.8	10.9
$\langle E_{trans} \rangle$ [f]	3.1	5.3	6.5	6.5	9.0	10.5	11.0	13.2
$\langle E_{int} \rangle$ [g]	0.6	0.6	0.6	1.05	1.05	1.05	1.04	1.05

[a] T_{HF} denotes the temperature of HF nozzle in degrees Kelvin.
[b] T_{Ba} denotes the temperature of barium oven in degrees Kelvin.
[c] P_{HF} is the pressure of HF behind nozzle in Torr.
[d] P_{H_2} is the pressure of H_2 behind nozzle in Torr.
[e] $\langle E_{beam} \rangle$ is the average beam energy in kcal/mole.
[f] $\langle E_{trans} \rangle$ is the average collision energy in kcal/mole.
[g] $\langle E_{int} \rangle$ is the average internal energy (rotation) of HF in kcal/mole.

$$v = (5RT_{nozzle}/M_{mean})^{1/2} , \qquad (3)$$

where R is the gas constant. The HF beam energies calculated from Eq. (3) agree well with the average HF beam energies obtained from the time of flight experiments described in Appendix A. This result, indicating a lack of substantial rotational relaxation, is not surprising since both HF and H_2 have extremely large rotational spacings. Hydrogen is used as the carrier gas in some experiments rather than helium since it is lighter and thus allows the attainment of higher beam energies.

Being the lighter collision partner, the fast HF predominantly controls the collision energy. The distribution of collision energies between Ba and HF has some breadth about the average collision energy for a number of reasons: (i) The nozzle expansion conditions are mild, yielding a finite Mach number, i.e., a distribution of velocities about the average velocity calculated from Eq. (3). The average Mach number, obtained from the time of flight experiments, is $\mathfrak{M} = 4.2$, but this is likely to be an underestimate because of the experimental factors described in Appendix A. (ii) There is a distribution of Ba velocities from the effusive oven operated near 1200 °K. (iii) Because of the substantial angular divergence of the two beams, there is a distribution of collision angles in the lab frame. The convolutions necessary to obtain a distribution of collision energies were carried out numerically and are described in Appendix B. We list in Table I, the experimental conditions and the average collision energies attained for eight different experiments performed. These eight are representative of a large number of experimental runs done on different days.

D. HF beam flux

In order to measure the reaction cross section as a function of collision energy, it is necessary to know the HF beam intensity as the seeding ratio is varied. For this purpose the HF beam flux is sampled at the crossing region with a quadrupole mass spectrometer (UTI Model 100B). The mass spectrometer is differentially pumped by a 2 in. diffusion pump. Figure 2

shows the measured HF beam flux as a function of the mole fraction of carrier gas for different experimental conditions. As the fraction of carrier gas increases, the HF beam intensity also increases because of Mach number focusing, [14] in which the heavier species are concentrated in the central portion of the beam. At high concentrations of carrier gas the beam intensity decreases again due to scattering both in the source chamber and to a lesser extent in the scattering chamber.

The role of HF dimers was investigated but found not to contribute to the observed BaF signal. The same relative collision energy can be obtained in two ways: (i) by using a low temperature (300 °K) and a large fraction of carrier gas; and (ii) by using a high temperature (500 °K) and a small fraction of carrier gas. Although the first condition favors dimer formation compared to the second condition, we found no measurable difference in the observed product internal state distribution. [15] This result may not be surprising since the 6 kcal/mole binding energy[15] of the HF dimer may inhibit reaction with Ba.

III. RESULTS

A. Energy disposal in products

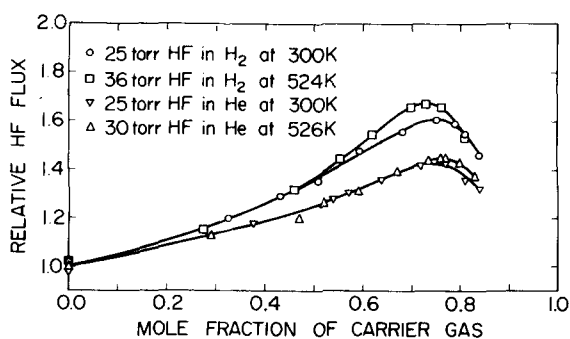Figure 3 presents typical excitation spectra for the reaction Ba + HF → BaF + H as a function of collision en-

FIG. 2. HF beam flux as a function of the carrier gas mole fraction in the expansion mixture.
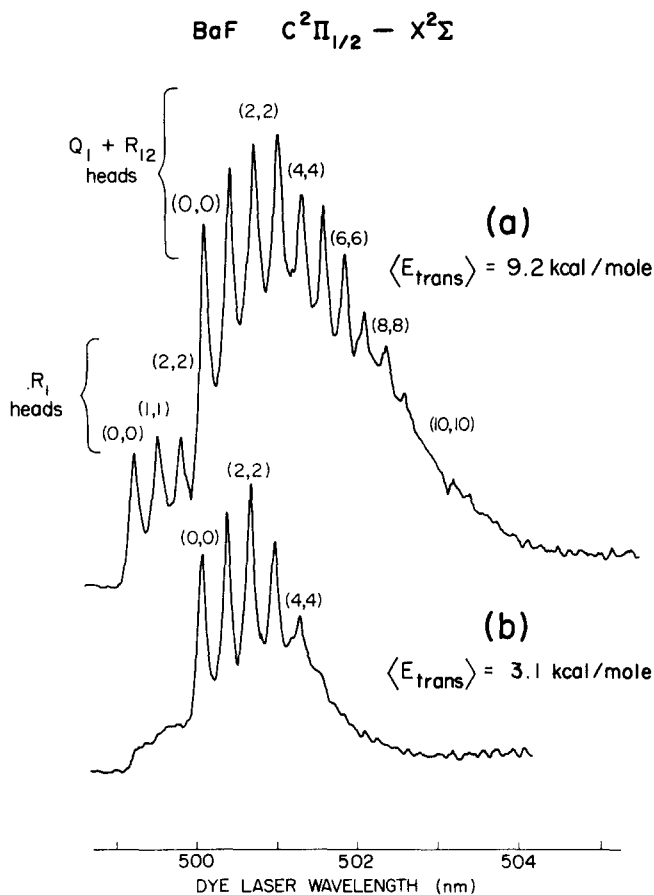
BaF $C^2\Pi_{1/2} - X^2\Sigma$

FIG. 3. Excitation spectra of the BaF product formed in the reaction Ba + HF for two different average collision energies $\langle E_{trans}\rangle$.

ergy. The qualitative difference between the excitation spectrum at high energy [Fig. 3(a)] and at low energy [Fig. 3(b)] is striking. While the low energy spectrum is similar to that obtained previously in a thermal beam–gas arrangement,[2] the high energy spectrum shows the appearance of new features.

To understand the nature of the BaF $C^2\Pi - X^2\Sigma^+$ excitation spectra, it is necessary to review briefly the formation of band heads.[16] A $^2\Pi - ^2\Sigma^+$ band system has a total of 12 branches, six belonging to each subsystem, $^2\Pi_{1/2} - ^2\Sigma^+$ and $^2\Pi_{3/2} - ^2\Sigma^+$. Spin–orbit interaction splits the $^2\Pi_{1/2}$ and $^2\Pi_{3/2}$ states. For the BaF C state, the spin–orbit constant ($A = 195.6$ cm^{-1}) is large and thus the two subsystems are well separated. The line positions of each branch may be represented to good approximation by a quadratic polynomial in the rotational quantum number J. If the coefficient of the term linear in J has a sign opposite to the coefficient of the term quadratic in J, then with increasing J the line positions approach a limiting value, the band head, and then turn back upon themselves. This causes the intensity to fall abruptly at the turning point but to decrease more gradually in the other direction. For the BaF $C^2\Pi_{1/2} - X^2\Sigma^+$ subsystem, the effective rotational constant[2] of the upper state $B^{(1)}_{eff}$ is less than the rotational constant of the lower state B''. This causes bandheads to appear in three of the six branches, the Q_1 and R_{12} branches at

almost the same frequency and value of J,

$$J^{Q_1 + R_{12}}_{head} = \tfrac{1}{2} B^{(1)}_{eff} / (B'' - B^{(1)}_{eff}) , \qquad (4)$$

and in the R_1 branch at higher frequency and at a value of J three times that of the $Q_1 + R_{12}$ head, i.e.,

$$J^{R_1}_{head} = 3 J^{Q_1 + R_{12}}_{head} . \qquad (5)$$

The rotational constants depend on the vibrational level. However, for the (0, 0) band of the $C^2\Pi_{1/2} - X^2\Sigma^+$ transition, $J^{Q_1 + R_{12}}_{head} \approx 37$ and $J^{R_1}_{head} \approx 110$.[17] Thus, a head in the R_1 branch will only appear if high rotational levels are populated.

The BaF $C - X$ system behaves like the other visible band systems of the alkaline earth monohalides, namely, almost all the intensity appears in the $\Delta v = 0$ sequence for low values of the vibrational quantum number v. This allows us to identify directly the (0, 0), (1, 1), (2, 2), ··· band heads of the $Q_1 + R_{12}$ branches, as indicated in Fig. 3. Moreover, because the Franck–Condon factors of these bands are nearly unity, the relative vibrational populations may be roughly estimated at a glance. Hence, we conclude from Fig. 3 that increasing collision energy causes population of higher vibrational levels of the BaF product. A comparison of Figs. 3(a) and 3(b) reveals that the former has additional band heads to the blue of the $Q_1 + R_{12}$ head of the (0, 0) band. These are identified as the R_1 band heads of the $\Delta v = 0$ sequence, which are shown more clearly in the high resolution trace of Fig. 4. Because these heads can only be formed when high rotational levels are populated, it is also possible to conclude from only a cursory inspection of Figs. 3 and 4 that increasing collision energy causes significant rotational excitation of the BaF product.

To make quantitative estimates of the product internal state distribution, a computer program was written to simulate the observed excitation spectra. The program, based on previous work by Karny, Estler, and Zare,[18] calculates the line positions for the six branches of each band using the spectroscopic constants given in Table II by means of standard formulas.[16] As input one estimates the relative vibrational and rotational populations. The latter are assumed to have the form
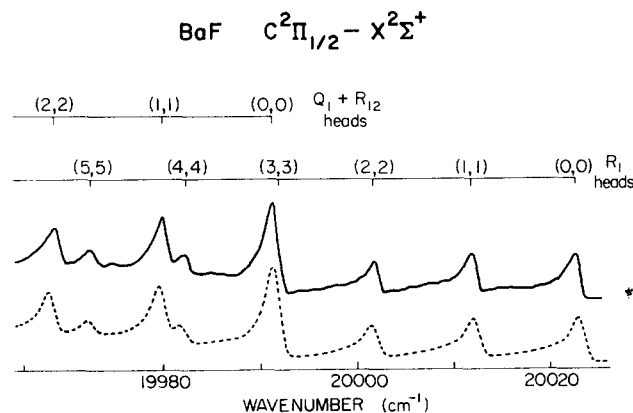
BaF $C^2\Pi_{1/2} - X^2\Sigma^+$

FIG. 4. High resolution portion (0.04 nm bandwidth) of the BaF excitation spectrum for the reaction Ba + HF with an average collision energy of $\langle E_{trans}\rangle = 13.2$ kcal/mole. The dashed curve is a computer simulation.

TABLE II. Spectroscopic constants (cm^{-1}) of BaF used for simulation of the excitation spectra.

Constants[a]	$X\,^2\Sigma^+$	$C\,^2\Pi_{1/2}$
T_e	0	19 993.719
ω_e	470.072	457.913
$\omega_e x_e$	1.717	1.559
$\omega_e y_e$	−0.032 97	−0.036 89
$\omega_e z_e$	+0.000 978	+0.001 16
B_e[b]	0.216 44[e]	0.213 48[d]
α_e	0.001 17[e]	0.001 064[d]

[a]The vibrational constants are taken from Ref. 19. The value of $\omega_e z_e$ for the X state was misprinted, but recalculated using Column 3 of Table II of Ref. 19.
[b]For the X state the value given is B_e, but for the C state it is $(B_e^{(1)})_{\text{eff}} = B_e(1-B_e/A)$. The program uses the approximation, $(B_v^{(1)})_{\text{eff}} = (B_e^{(1)})_{\text{eff}} - \alpha_e(v+\tfrac{1}{2})$.
[e]Reference 2.
[d]We adjusted these two values to obtain the best fit to the band head positions of our experiment No. 8 (shown in Fig. 4).

$$P(J\,|\,v) = N_v P^0(J\,|\,v) \exp[-f_R\,\theta_R^v/(1-f_V)] , \qquad (6)$$

which gives a linear rotational surprisal.[20] Here N_v is a normalization factor, $P^0(J\,|\,v)$ is the "prior" distribution

$$P^0(J\,|\,v) = (2J+1)(1-f_V-f_R)^{1/2} , \qquad (7)$$

which reflects the density of states without angular momentum constraints, f_V and f_R are the fractions of the total energy[21] as vibration and rotation in the product $(v,\,J)$ level, and θ_R^v is an adjustable parameter. Each line is weighted not only by the population of the initial $(v,\,J)$ level but also by the Franck–Condon factor[22] and the rotational line strength[23] of the pump transition. At each frequency, the program convolutes each line with the laser bandwidth to produce a simulated spectrum. The bandwidth is assumed to be of the form of a Gaussian having a full width at half maximum of 0.04 nm. Because the laser intensity is observed to be constant over the range of the spectrum, no correction is made for its variation with wavelength.

The simulated spectrum is compared visually to the observed spectrum and new estimates are made of the vibrational populations and the rotational parameters θ_R^v. This procedure is iterated typically four to six times to achieve a good fit. The dashed curve in Fig. 4 is a simulated excitation spectrum obtained in this manner.

Table III lists the values of the relative vibrational cross section $\sigma(v)$ and the rotational parameter θ_R^v, found by computer simulation for eight different experimental conditions. Also shown in Table III are the average energies into product vibration $\langle E'_{\text{vib}} \rangle$ and product rotation $\langle E'_{\text{rot}} \rangle$, calculated from the values of $\sigma(v)$ and θ_R^v. The average energy in product translation $\langle E'_{\text{trans}} \rangle$ is found by difference from the total energy available to the products $\langle E'_{\text{tot}} \rangle$. The latter is the sum of the reaction exothermicity[21] $-\Delta H^0_0 = 4.4 \pm 1.6$ kcal/

mole, and the reagent translational and internal energies (Table I).

Figure 5 illustrates how the microscopic cross sections $\sigma(v)$ change with collision energy. The vibrational distribution of the product peaks near $v = 0$, 1 for low collision energies [Fig. 5(a)], peaks at higher vibrational levels at intermediate collision energies [Fig. 5(b)], and peaks once again at $v = 0$ for the highest collision energies we studied [Fig. 5(c)]. Note that as the collision energy increases, the breadth of the vibrational distribution also increases, extending to or nearly to the highest vibrational level energetically accessible (marked by arrows in Fig. 5).

Table IV presents the average rotational energy in each vibrational level for the different collision energies studied. These are computed from Eq. (6) using the values of θ_R^v given in Table III. In many cases the parameters θ_R^v are set equal to one another beyond some value of v. For the lower vibrational levels, the average rotational energy is approximately constant, but decreases monotonically for higher vibrational levels. While the average rotational energies are determined more accurately for the lower vibrational levels where the R_1 band heads are observed, those for the higher vibrational levels become increasingly constrained by the total energy available to the products.
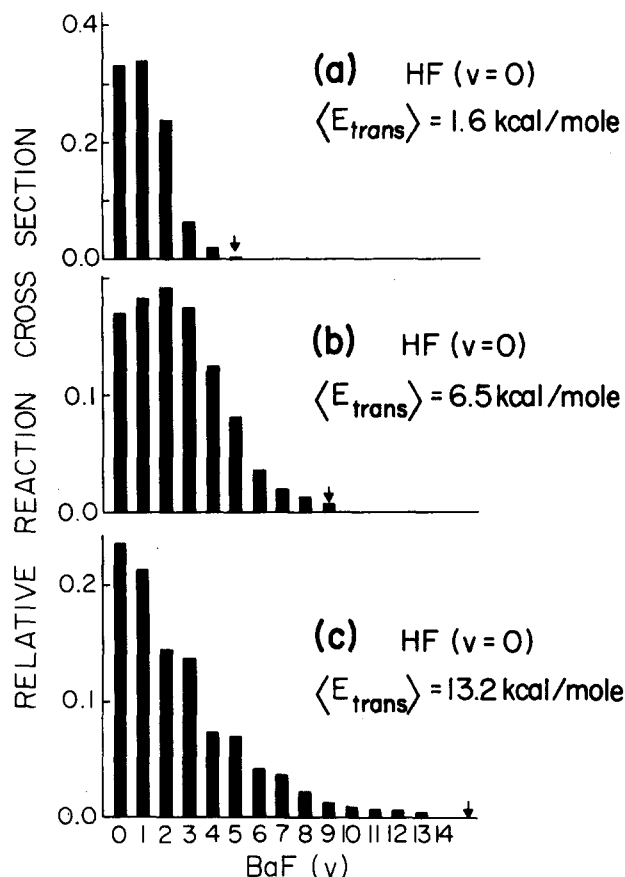

FIG. 5. Relative cross sections $\sigma(v)$ for producing BaF(v) under various reagent conditions: (a) from a reanalysis of Fig. 3 in Ref. 2; (b) from experiment 4 and (c) from experiment 8. An arrow marks the highest BaF vibrational level energetically accessible for each reagent condition.

TABLE III. Product internal state distributions. The first entry denotes the microscopic cross section $\sigma(v)$, for formation of product in vibrational level v; the second entry is the rotational fitting parameter θ_R^V as a function of collision energy.

v	Expt. No. $\langle E_{trans} \rangle$	1 3.1	2 5.3	3 6.5	4 6.5	5 9.0	6 10.5	7 11.0	8 13.2
0		0.214	0.194	0.175	0.170	0.217	0.214	0.239	0.234
		2.2	1.4	1.1	1.0	0.6	1.3	1.4	0.7
1		0.272	0.213	0.185	0.182	0.178	0.194	0.211	0.211
		0.8	0.7	0.7	0.6	0.0	0.8	0.7	0.6
2		0.302	0.215	0.195	0.191	0.164	0.158	0.156	0.142
		0.2	−0.1	0.0	−0.1	−0.1	−0.1	−0.2	0.3
3		0.163	0.179	0.180	0.174	0.126	0.135	0.132	0.135
		−0.3	−0.2	−0.2	−0.2	−0.4	−0.5	−0.6	−0.5
4		0.042	0.117	0.136	0.123	0.101	0.104	0.088	0.072
		−0.6	−0.5	−0.3	−0.3	−0.7	−0.8	−0.7	−0.7
5		0.007	0.055	0.082	0.082	0.089	0.075	0.069	0.069
		−0.8	−0.5	−0.5	−0.5	−0.8	−0.8	−0.8	−0.8
6			0.017	0.033	0.036	0.052	0.051	0.039	0.041
			−0.5	−0.5	−0.5	−0.8	−0.9	−0.8	−0.8
7			0.009	0.014	0.019	0.034	0.031	0.027	0.036
			−0.5	−0.5	−0.5	−0.8	−0.9	−0.8	−0.8
8					0.013	0.016	0.167	0.019	0.019
					−0.5	−0.8	−0.9	−0.8	−0.8
9					0.010	0.009	0.008	0.006	0.012
					−0.5	−0.8	−0.9	−0.8	−0.8
10						0.008	0.007	0.006	0.008
						−0.8	−0.9	−0.8	−0.8
11						0.005	0.005	0.006	0.006
						−0.8	−0.9	−0.8	−0.8
12									0.005
									−0.8
13									0.005
									−0.8
$\langle E'_{tot} \rangle$		8.1	10.3	11.5	12.0	14.5	15.9	16.5	18.7
$\langle E'_{vib} \rangle$		2.1	2.8	3.1	3.35	3.45	3.4	3.1	3.4
$\langle E'_{rot} \rangle$		2.1	2.8	3.2	3.35	4.45	4.8	5.1	5.9
$\langle E'_{trans} \rangle$		3.9	4.7	5.2	5.3	6.6	7.7	8.3	9.4

TABLE IV. Average product rotational energy $\langle E'_{rot} \rangle_v$ in each product vibrational level v. All energies are in kcal/mole.

v	Expt. No. $\langle E_{trans} \rangle$	1 3.1	2 5.3	3 6.5	4 6.5	5 9.0	6 10.5	7 11.0	8 13.2
0		2.2	3.2	3.8	4.0	5.2	5.0	5.2	6.6
1		2.3	3.2	3.6	3.8	5.3	5.1	5.4	6.2
2		2.1	3.1	3.5	3.8	4.8	5.4	5.7	6.1
3		1.7	2.6	3.1	3.3	4.5	5.2	5.5	6.4
4		1.2	2.2	2.6	2.8	4.1	4.9	5.0	6.0
5		0.7	1.6	2.2	2.4	3.6	4.3	4.5	5.5
6			1.1	1.6	1.8	3.0	3.7	3.9	4.9
7			0.5	1.1	1.2	2.5	3.2	3.4	4.4
8				0.5	0.7	1.9	2.6	2.8	3.8
9					0.2	1.3	2.0	2.2	3.2
10						0.8	1.4	1.7	2.7
11						0.2	0.9	1.1	2.1
12									1.6
13									1.0

The state-to-state reaction rates summarized in Table III are displayed graphically in the form of triangular contour plots[24] (Fig. 6). One sees readily that the highest contour of reactivity moves from near the lower left-hand corner ($f'_V = 0.2$, $f'_R = 0.18$, $f'_T = 0.62$) at low collision energies [Fig. 6(a)] to a more central location ($f'_V = 0.22$, $f'_R = 0.41$, $f'_T = 0.37$) at intermediate collision energies, and then finally returns to the TR baseline ($f'_V = 0.0$, $f'_R = 0.35$, $f'_T = 0.65$) at 13.2 kcal/mole collision energy [Fig. 6(c)].

It is also useful to describe the reaction by the fractional energy disposed into each product mode, as shown in Fig. 7. At a glance, one notices that at low collision energies $\langle f'_{vib} \rangle$ and $\langle f'_{rot} \rangle$ nearly coincide while $\langle f'_{trans} \rangle$ is larger than either. Closer inspection reveals that $\langle f'_{vib} \rangle$ increases with collision energy to a maximum and then decreases, while $\langle f'_{trans} \rangle$ exhibits a corresponding minimum. The change of $\langle f'_{rot} \rangle$ with increasing collision energy is a gradual increase that levels off at the highest energies studied. In previous work,[2] $\langle f'_{trans} \rangle$ was estimated to be too high because the heat of reaction was calculated from an inaccurate value
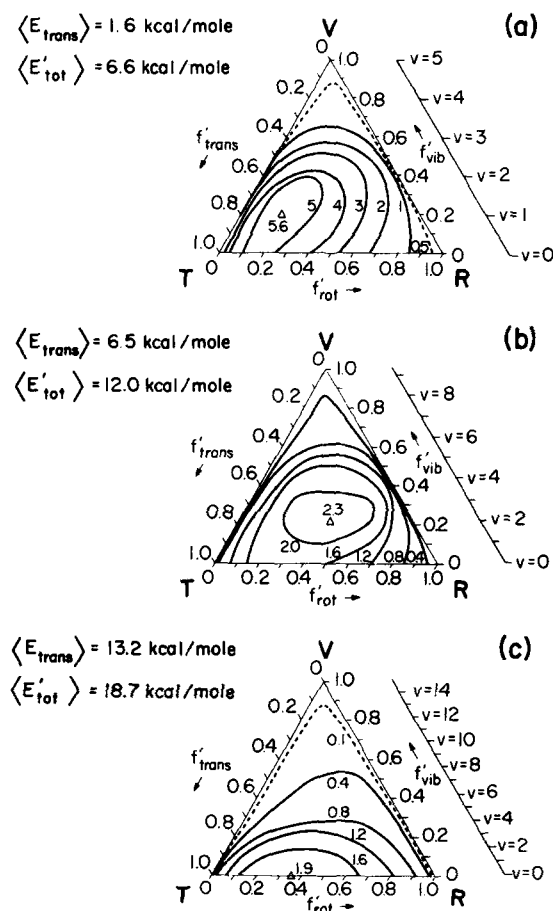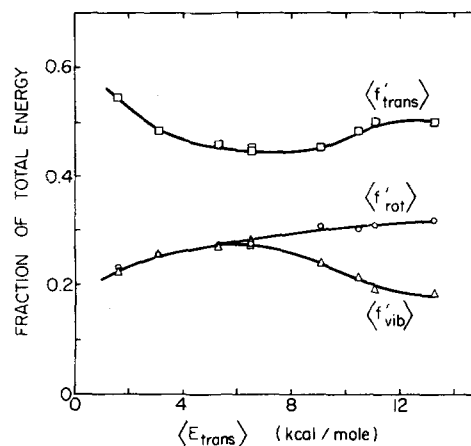

FIG. 7. Fractional energy disposal as a function of average collision energy.

of the BaF bond energy. Nonetheless, the Ba + HF reaction is rather remarkable in that product translation dominates over the other two modes in the disposal of energy.

B. Dependence of reaction cross section on collision energy

The total cross section for the formation of BaF in the crossed beam reaction Ba + HF is determined by[5]

$$\sigma = F_{BaF} / n_{Ba} n_{HF} \, \Delta V v_{rel} , \qquad (8)$$

where F is flux, n is number density, ΔV is the reaction volume, and v_{rel} is the relative reagent velocity. The subscripts indicate the species concerned. We use the relations $n_{HF} = F_{HF} / v_{HF}$ and $F_{BaF} = n_{BaF} v_{BaF}$, which for this mass combination becomes $F_{BaF} \simeq n_{BaF} v_{c.m.}$. Then Eq. (8) may be rewritten

$$\sigma = n_{BaF} \left(\frac{1}{F_{HF}} \right) \left(\frac{v_{c.m.} v_{HF}}{v_{rel}} \right) \left(\frac{1}{n_{Ba} \Delta V} \right) , \qquad (9)$$

where $v_{c.m.}$ is the center of mass velocity and v_{HF} and v_{BaF} are lab velocities. The expression for σ in Eq. (9) has been represented as the product of four factors. The first factor n_{BaF} is proportional to the integrated BaF fluorescence intensity; the second factor has been measured (see Fig. 2); the third factor is calculated from the known reagent conditions; and the fourth factor is constant since the reaction volume is unchanged for different runs (Mach focusing[14] does not appreciably affect ΔV for our geometry). By evaluating Eq. (9) for different reagent conditions, the relative total cross section has been determined as a function of collision energy (Fig. 8).

Although Reaction (1) is exothermic, the reaction cross section increases with collision energy, reaching a maximum near 6 to 8 kcal/mole. This implies a small activation energy E_a. The data in Fig. 8 are deconvoluted from the distribution of experimental collision energies, discussed in Appendix B, by assuming a functional form for the dependence of the cross section on translational energy. We choose the model[25,26]

$$\sigma(E_{trans}) \propto (E_{trans} - E_0)^s / E_{trans} , \qquad (10)$$

FIG. 6. Contours of equal reaction cross section into product internal (v, J) states for different reagent collision energies. The coordinates of each point represent the fractional energy released into product vibration f'_{vib}, rotation f'_{rot}, and translation f'_{trans}. Note that near the apex V, R, or T, most of the energy appears in that product mode. For reference a scale of product vibrational quantum numbers is indicated in each case.
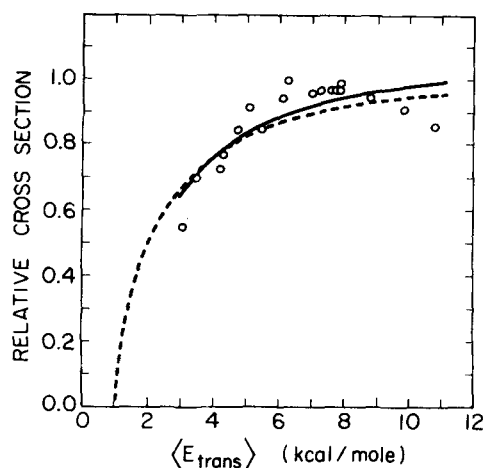
FIG. 8. Relative cross section for Reaction (1) as a function of the average collision energy. The open circles are the experimental data. The solid curve is the best fit to the experimental data assuming the line of centers model. It is obtained by convolution of the dashed curve [$s = 1$, $E_0 = 1.0$ kcal/mole in Eq. (10)] with the collision energy distribution at each energy (see Fig. 12).

where E_0 is the threshold energy and s is a positive real number. When $s = 1$, Eq. (10) corresponds to the line of centers model.[25] A least-squares fit to this model yields $E_0 = 1.0$ kcal/mole. When both s and E_0 are allowed to vary, the best fit is obtained for $E_0 = 2.3$ kcal/mole and $s = 0.6$. From this fitting procedure we can only state with confidence that the threshold energy is between 1 and 3 kcal/mole.

The activation energy E_a may be related to the threshold energy E_0 provided the dependence of the total cross section on translational energy is known.[27] For Eq. (10) it follows that

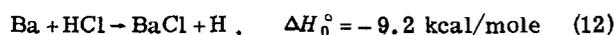$$E_a = E_0 + (s - \tfrac{1}{2})RT \ , \tag{11}$$

which is a generalization of previous results.[27] The presence of a finite activation energy selects the higher energy reagents and therefore makes more average energy available to the products.

No activation energy was included in calculating values of $\langle E'_{tot} \rangle$ in Table III. A substantial threshold of ~3 kcal/mole would necessarily increase $\langle E'_{tot} \rangle$ for the thermal experiments [Fig. 6(a)], making about two more product vibrational levels accessible. Such levels are not observed, and it is therefore likely that the threshold is closer to 1 kcal/mole, consistent with the results for the line of centers model.
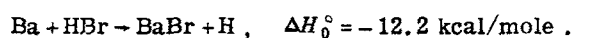
IV. DISCUSSION

A. Fate of reagent translational energy

Previously, Schultz and Siegel[10] have studied the dependence of product internal state distribution upon collision energy for the exothermic reactions

$$Ba + HCl \rightarrow BaCl + H \ , \qquad \Delta H_0^\circ = -9.2 \text{ kcal/mole} \tag{12}$$

and

$$Ba + HBr \rightarrow BaBr + H \ , \qquad \Delta H_0^\circ = -12.2 \text{ kcal/mole} \ . \tag{13}$$

The present work adds another member to this chemical family and presents an opportunity to investigate how the dynamics vary from one member to another.

For a number of systems Polanyi and co-workers[6] have found that excess collision energy above the barrier ΔE_{trans} leads to extra translational and rotational energies in the products, i.e.,

$$\Delta E_{trans} \rightarrow \Delta E'_{trans} + \Delta E'_{rot} \ . \tag{14}$$

To test this generalization for Reaction (1), we compare the results under thermal conditions [Figs. 5(a) and 6(a)] to those obtained at the highest collision energy (experiment 8). The extra reagent energy ($\Delta E_{trans} = 11.6$ kcal/mole; $\Delta E_{rot} = 0.5$ kcal/mole is distributed among the products as follows: $\Delta E'_{vib} = 16\%$, $\Delta E'_{trans} = 48\%$, and $\Delta E'_{rot} = 36\%$. Thus it is clear that Eq. (14) is at least qualitatively true. However, since there is a change of behavior near $E_{trans} = 6$ to 8 kcal/mole, as shown in Fig. 7, it is instructive to examine this relation in more detail. In comparing the thermal experiment with experiment 3 we find the additional energy ($\Delta E_{trans} = 4.9$ kcal/mole; $\Delta E_{rot} = 0$) is distributed as $\Delta E'_{vib} = 33\%$, $\Delta E'_{trans} = 33\%$, and $\Delta E'_{rot} = 33\%$. In the higher energy range, a comparison of experiment 4 with experiment 8 shows that the additional energy ($\Delta E_{trans} = 6.7$ kcal/mole; $\Delta E_{rot} = 0$) is distributed as $\Delta E'_{vib} = 1\%$, $\Delta E'_{trans} = 60\%$, and $\Delta E'_{rot} = 39\%$. Therefore, we find that Eq. (14) is obeyed rather poorly in the low energy regime ($E_{trans} < 6.5$ kcal/mole) where the excess energy appears to be equally distributed among all modes, but is followed almost quantitatively in the high energy regime. This suggests that a transition takes place between two reaction mechanisms in the range 6–8 kcal/mole. Further support for this interpretation is provided by Fig. 8 which shows that the collision cross section reaches a maximum in this region. This may help explain the change in the fractional disposal of energy (Fig. 7) which exhibits extrema in the same energy range.

For Reactions (12) and (13), the product vibrational distributions remain nearly unchanged with increasing collision energy.[10] Almost all the extra reagent energy is channelled into product translation and rotation, in good accord with Eq. (14). This is in contrast to the Ba + HF reaction which shows a change in behavior near 6 to 8 kcal/mole.

We do not understand at this time why Eq. (14) is poorly satisfied at low collision energies for the Ba + HF reaction, but we speculate that it is related to the presence of secondary encounters between the reacting species.[28] These complex trajectories may couple the reagent modes, vibration and translation, causing the disposal of excess energy in the product modes to be more equally partitioned. At higher collision energies, such snarled trajectories may be less important.

B. Relation between product rotation and reaction cross section

Reactions (1), (12), and (13) have the mass combination

$$H + HL \rightarrow HH + L \ , \tag{15}$$

where H and L represent heavy and light atoms. This class of reactions is kinematically constrained[29] in that the reagent orbital angular momentum L is effectively carried over into product rotation J':

$$J' \sim L \equiv \mu v_{rel} b \qquad (16)$$

Here μ is the reduced mass of the reagents approaching with a relative velocity v_{rel} at an impact parameter b. The light atom L (in our case, hydrogen) is unable to carry away much angular momentum as compared to its heavier partner. The validity of Eq. (16) is supported by classical trajectory calculations on a number systems.[10,30] When Eq. (16) is obeyed, a measurement of the product rotational distribution (J') at a given collision velocity (v_{rel}) provides information about the range of impact parameters (b) that lead to reaction. From the latter one can place a limit on the total reaction cross section since $\sigma \lesssim \pi b_{max}^2$, where b_{max} is the maximum reactive impact parameter. The equality obtains only if all collisions with $b \lesssim b_{max}$ lead to reaction.

We use the phase space theory of Pechukas and Light[31,32] to model our reaction, particularly the product rotational distributions, because this treatment incorporates the conservation of angular momentum. Phase space calculations yield complete product energy distributions on the assumption that every product state is equally probable given the constraints of energy and angular momentum conservation. These calculations allow us to judge the extent to which the experimental product distribution is fit by a statistical model. It also permits a realistic estimate to be made of the product rotational distribution for this mass combination. This estimate will reflect the actual product rotational distribution provided that Eq. (16) holds and that the reactivity as a function of impact parameter (the opacity) is approximately constant for $b \lesssim b_{max}$.

Using the phase space computer program described by Dagdigian et al.,[33] the average product rotational

TABLE V. Results of phase space calculation.

Collision Energy (kcal/mole)	3.1	6.5	13.2
J_i[a] ($\hbar$)	3	4	4
L_{max} ($\hbar$)	88	110	148
b_{max} (Å)	2.66	2.28	2.15
b_{max}^2 (Å^2)	22.2	16.4	14.6
$\langle E_{rot}' \rangle$[b] (kcal/mole)	2.1	3.35	5.9
$\langle E_{vib}' \rangle$[c] (kcal/mole)	1.9	3.0	4.5
$\langle E_{vib}' \rangle_{expt}$[d] (kcal/mole)	2.1	3.35	3.4

[a]Rotational level of the reagent molecule (HF) for which calculation has been done. The rotational energy for this level matches approximately with the average rotational energy for the corresponding experiment.
[b]The average energy going into product rotation. This has been forced to match the experimental result.
[c]Average energy going into product vibration as calculated from theory.
[d]Average energy going into product vibration as obtained experimentally (see Table III).
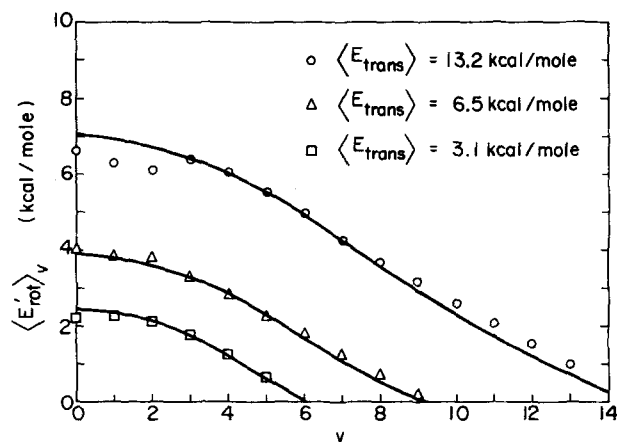

FIG. 9. Average rotational energy in a given product vibrational level, $\langle E_{rot}' \rangle_v$ as a function of the vibrational level. Points are experimental values and the curves are calculated from phase space theory.

energies $\langle E_{rot}' \rangle$ were calculated for a number of collision energies but found to be about a factor of 2 higher than the experimental values. This calculation[34] assumed a cutoff value for the orbital angular momentum L_{max} based on an attractive potential of the form $C^{(6)} r^{-6}$. To circumvent this difficulty, we chose to set L_{max} at a value such that the calculated average product rotational energy matches the experimental result. The form of the exit channel was unchanged, although the $C^{(6)}$ potential is not likely to be an appropriate description. However, tests showed that the results of this calculation (Table V) were quite insensitive to the potential in the exit channel.

Table V shows that the phase space model does not give an accurate representation of the average energy going into product vibration $\langle E_{vib}' \rangle$, although the variation with collision energy is correct. Moreover, the calculated values of $\sigma(v)$ (not shown) decrease monotonically with increasing v at all collision energies, which is at variance with the experimental results (see Fig. 5). However, the calculated average energies in product rotation for each vibrational level agree remarkably well with the experimental values (Fig. 9). Indeed, the shape of the experimental and theoretical curves coincide within the uncertainty in the experimental data. Actually the analysis of the experimental data may overestimate the population in high J' values because the use of Eq. (7) does not take into account angular momentum conservation. This should have less of an effect on the average rotational energy in a vibrational level. The close agreement in Fig. 9 does not necessarily indicate that the Ba + HF reaction proceeds through a long-lived complex yielding a statistical outcome; instead, the agreement reflects the validity of Eq. (16) and the assumption that the opacity function is nearly constant for $b \lesssim b_{max}$.

The values of πb_{max}^2 given in Table V are upper bounds to the reaction cross section. Notice however that πb_{max}^2 decreases with increasing collision energy, in contradiction to the experimental data (Fig. 8). This discrepancy implies that at least at low collision energies not all collisions with $b \lesssim b_{max}$ are reactive. We intro-

duce a steric factor $p \equiv \sigma/\pi b_{max}^2$, which increases with collision energy. If the steric factor reaches unity at high collision energies, then the value of the cross section for Reaction (1) is estimated to be about 15 Å^2 at $\langle E_{trans} \rangle = 13.2$ kcal/mole. This value is then an upper bound to the reaction cross section.

Siegel and Schultz[10] have carried out classical trajectory calculations on Reaction (12) using a number of different potential energy surfaces. In all cases they find Eq. (16) to hold and, moreover, that the reaction probability is unity for $b \lesssim b_{max}$, i.e., $p = 1$. Our results on Reaction (1) also are consistent with Eq. (16) but show that p is not always unity as discussed above. Three factors may contribute to this difference: (a) Reaction (1) has a higher barrier than Reaction (12); (b) Reaction (1) is a less extreme example of the mass combination (15) than Reaction (12); and (c) the trajectory calculations of Schultz and Siegel neglected the zero point vibrational motion and hence the vibrational phase of the HCl molecule.

C. Nature of the Ba + HF potential energy surface

The present study provides a wealth of information on the Ba + HF reaction system. Ideally, one wishes to compare these results to the prediction of dynamical calculations based on reliable potential energy surfaces. Unfortunately, the construction of such surfaces involving heavy atoms is presently in a developmental state. We content ourselves here to a discussion of general features of the Ba + HF surface that can be inferred from available data.

This reaction system has the curious property that its reaction exothermicity of 4.4 ± 1.6 kcal/mole is caused entirely by the large change in zero point energy $G(0)$ in going from HF $[G(0) = 5.85$ kcal/mole] to BaF $[G(0) = 0.67$ kcal/mole]. Thus the electronic surface from bottom of the entrance well to the bottom of the exit well may even be slightly endothermic by 0.8 ± 1.6 kcal/mole. Although an early barrier is thought to be a general characteristic of exothermic reactions,[35] for Ba + HF the barrier is not so constrained since the surface is nearly thermoneutral. The variation of zero point energy along the minimum energy path will be important in determining the location of the barrier. The present data indicates that the barrier height must be on the order of 1 kcal/mole for this reaction. Because the fraction of total energy that appears in product vibration is unusually small, it appears that the energy release is extremely repulsive.[2,36] The lack of "mixed" energy release which is ordinarily favored by this mass combination,[35] suggests a later barrier than is common for exothermic reactions.

The nature of the entrance channel is determined in part by the maximum value of L that contributes to reaction (Table V). The effective potential is the sum of the potential for $L = 0$ and the centrifugal correction $L^2/2\mu r^2$. For encounters with angular momentum L_{max} the effective potential equals E_{trans}, giving information about the potential for $L = 0$.

Because of the switch of predominantly covalent bond-

ing in HF to ionic bonding in BaF, the LEPS-type potential may be inadequate in describing this reaction.[36] The alkaline earth atoms have divalent character and one expects that HBaF will be strongly bound with respect to any of its diatomic constituents. It is unclear whether any reactive encounters sample this region of the potential energy surface but bent configurations may be important, as suggested by studies[18] of the Sr + HF reaction using oriented HF molecules.

The present studies are indicative of the detailed dynamical data that now can be obtained in favorable cases using laser induced fluorescence as a product detector. The results provide stringent tests for the construction of accurate reactive scattering surfaces, which are underway in several laboratories.

ACKNOWLEDGMENTS

APPENDIX A: TIME OF FLIGHT MEASUREMENTS OF THE SEEDED HF BEAM

Time of flight analysis is employed to determine the velocity distribution of the HF beam and to check the assumption that rotational relaxation does not affect the beam velocity [see Eq. (3)]. For the time of flight measurements, the HF beam is chopped by a two slit wheel (slit width, 1.0 mm; radius, 5.4 cm). A typical chopping frequency is 240 Hz. Fluorescence excited in BaF from the reaction of the chopped HF beam with Ba is used as the detection system. The barium metal oven is placed at a greater distance downstream than is the case in the main experiment. The path traversed by the HF beam from the chopping wheel to the interaction region is 15.7 cm. Time of flight velocity analysis using laser induced fluorescence detection has been reported previously by Pasternak and Dagdigian.[37] Our method is similar except that the fluorescence is excited in the BaF product after reaction with Ba. The slits are positioned on opposite sides of the chopper wheel so that a lamp photodiode combination provides a synchronizing pulse when the HF beam passes through the other slit. After frequency division to about 12 Hz, these pulses are fed into a scan delay generator (Keithley) which provides the trigger pulse for the laser. Fluorescence is excited using the (2, 2) band of the BaF C-X transition. By scanning the delay between the laser trigger and the synchronization pulse, the time of flight spectrum is obtained. Figure 10 shows some sample spectra.

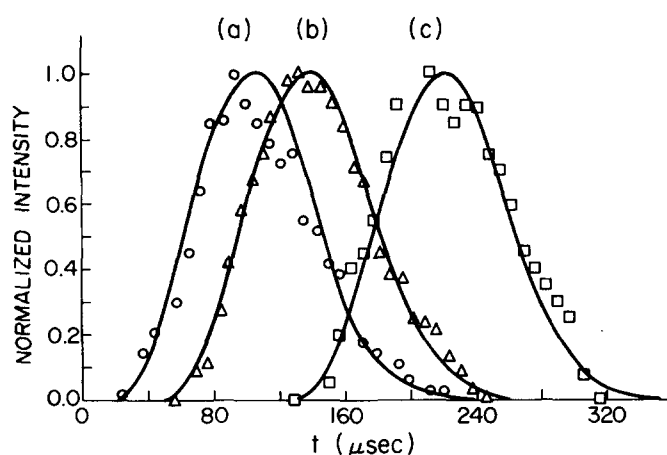The method used to analyze these spectra is described

FIG. 10. Normalized time of flight spectra for three different experimental conditions. The points represent experimental data. The solid line is the best fit to the points [Eq. (A1)].
(a) HF = 48 Torr, H_2 = 142 Torr, T_{nozzle} = 514 °K; (b) HF = 48 Torr, H_2 = 47 Torr, T_{nozzle} = 520 °K; (c) HF = 32 Torr, H_2 = 0 Torr, T_{nozzle} = 300 °K.

elsewhere.[38,39] A two parameter velocity distribution is assumed:

$$P(v) \propto (v/\alpha_s)^3 \exp[-(v-v_s)^2/\alpha_s^2] \ . \tag{A1}$$

The parameters v_s and α_s are related to the Mach number by the expression:

$$\mathfrak{M} = (N_s/\alpha_s)(2^{1/2}/\bar{\gamma}) \ . \tag{A2}$$

Here $\bar{\gamma}$ is the mean specific heat ratio. To obtain simulated time of flight spectra, Eq. (A1) was transformed into time space[38] and convoluted numerically with the detection system time constant and the chopper wheel gate function.[39] The time constant of the detection system is 20 μsec and is primarily due to the net rate of removal of BaF from the volume probed by the laser. See for example Fig. 5 of Ref. 12. The gate function is trapezoidal with a base of 110 μsec and a top of 50 μsec. A nonlinear least-squares fit yields the best values of v_s and α_s from which the Mach number may be calculated

from Eq. (A2). The results of the time of flight analysis are shown in Table VI. Average beam energies are computed and compared to those derived from Eq. (3). The average deviation is -0.2 kcal/mole, and the rms deviation is 0.6 kcal/mole. It is believed that most of the deviation is due to the scatter in the time of flight data. However, the higher values of the average beam energy as measured by the time of flight analysis at high concentration of H_2 carrier might be real and represent the onset of rotational cooling. Gallagher and Fenn[40] have investigated H_2 rotational relaxation in supersonic expansion and their results suggest that there is little rotational cooling over the range of operating conditions used in this study. Overall, the agreement between columns 7 and 9 of Table VI encourages us that Eq. (3) provides an adequate representation of the HF beam energy under our experimental conditions.

The spread in $\mathfrak{M}$ arises primarily from the fact that the apparatus time resolution accounted for a large fraction of the width of the measured time of flight spectra. Anderson and Fenn[41] have developed an empirical relation which predicts for the conditions used here Mach numbers in the range 6 ± 1. These are on the average higher than those obtained from our time of flight spectra but are within the scatter of the experimental data.

APPENDIX B: DISTRIBUTION OF COLLISION ENERGIES IN CROSSED MOLECULAR BEAM SCATTERING

To obtain a distribution of collision velocities and hence collision energies in a crossed molecular beam experiment, one must take into account the spread of (lab) velocities in each beam and the spread of angles (in the lab frame) at which the molecules collide. This problem was first solved by Datz, Taylor, and Herschbach[42] for the case of thermal beams. We generalize their results using the same notation.

We assume that the velocity distribution in each beam has the form of Eq. (A1), i.e.,

TABLE VI. Time of flight measurements.

| Nozzle conditions | | | | | Results | | | Calculation[e] | |
| Pressure | | | | | | | | | |
HF (Torr)	He/H_2 (Torr)	Temperature (°K)	α_s (10^5 cm/sec)	v_s (10^5 cm/sec)	$\mathfrak{M}$ Mach number	$\langle E_{beam}\rangle$[a] (kcal/mole)	$\langle E_{trans}\rangle$[b] (kcal/mole)	$\langle E_{beam}\rangle$[a] (kcal/mole)	$\langle E_{trans}\rangle$[b] (kcal/mole)
32	0	300	0.11	0.76	8.0	1.5	3.1	1.5	3.1
32	33 (He)	300	0.18	0.83	5.2	1.9	3.5	2.5	4.3
32	68 (He)	300	0.34	0.84	2.8	2.7	4.5	3.3	5.2
32	103 (He)	300	0.31	0.94	3.4	2.9	4.7	4.0	6.0
48	0	512	0.23	0.90	4.3	2.4	4.1	2.5	4.3
48	47 (He)	512	0.34	1.07	3.6	3.7	5.6	4.2	6.2
48	77 (He)	512	0.44	1.18	3.0	4.9	6.9	5.0	7.0
48	102 (He)	512	0.53	1.22	2.6	5.9	8.0	5.6	7.7
48	152 (He)	520	0.36	1.43	4.5	6.0	8.1	6.6	8.7
48	47 (H_2)	520	0.28	1.25	5.0	4.4	6.4	4.7	6.7
48	82 (H_2)	519	0.40	1.45	4.1	6.5	8.6	6.0	8.1
48	152 (H_2)	514	0.44	1.72	4.4	8.8	11.0	7.8	10.0

[a]Average beam energy.
[b]Average collision energy calculated numerically (Appendix B) assuming a barium oven temperature of 1200 °K.
[e]Calculated using Eq. (3).

$$P(v \mid \alpha_s, \ v_s) \propto (v/\alpha_s)^3 \exp[- (v - v_s)^2/\alpha_s^2] \ . \tag{B1}$$

For thermal beams, $v_s = 0$ and α_s is the rms velocity at the given temperature. We denote the velocities of the two beams by v_1 and v_2. These can be related to the magnitude and angle of the relative velocity vector v_{rel} and ψ (see Fig. 11). The transformation is

$$v_1 = v_{rel} \sin(\gamma + \psi)/\sin\gamma \tag{B2}$$

and

$$v_2 = v_{rel} \sin\psi/\sin\gamma \ , \tag{B3}$$

where γ is the angle at which the two beams intersect. The probability distribution for a collision velocity v_{rel} at an angle γ is given by[25,38,42,43]

$$P(v_{rel}, \ \gamma) dv_{rel} \propto \int_0^{\pi-\gamma} v_{rel} \ \frac{P(v_1 \mid \alpha_{s_2}, \ v_{s_1})}{v_1}$$

$$\times \frac{P(v_2 \mid \alpha_{s_1}, \ v_{s_2})}{v_2} \ J d\psi \, dv_{rel} \ , \tag{B4}$$

where

$$J = v_{rel} / \sin\psi \tag{B5}$$

is the Jacobian of the transformation. In Eq. (B4), $P(v)/v$ represents the number density and the integration is over all possible angles ψ of the relative velocity vector with respect to v_1. Substitution of (B1), (B2), (B3), and (B5) in (B4) yields[44]

$$P(v_{rel}, \ \gamma) dv_{rel} \propto \int_0^{\pi-\gamma} \frac{v_{rel}^6}{\sin^6\gamma} \sin^2\psi \, \sin^2(\gamma+\psi)$$

$$\times \exp\left[- \left(\frac{\sin(\gamma+\psi)}{\sin\gamma} \ \frac{v_{rel}}{\alpha_{s_1}} - \frac{v_{s_1}}{\alpha_{s_1}}\right)^2\right.$$

$$\left. - \left(\frac{\sin\psi}{\sin\gamma} \ \frac{v_{rel}}{\alpha_{s_2}} - \frac{v_{s_2}}{\alpha_{s_2}}\right)^2\right] d\psi \, dv_{rel} \ . \tag{B6}$$

Finally, one must integrate over the collision angles γ,

$$P(v_{rel}) dv_{rel} = \int_{\gamma_{min}}^{\gamma_{max}} A(\gamma) P(v_{rel}, \ \gamma) d\gamma \, dv_{rel} \ , \tag{B7}$$

where $A(\gamma)$ is the distribution of collision angles.

For our beam geometry, we take $A(\gamma)$ to be a triangular function between $108°$ and $163°$, peaking at $135°$. The Ba beam is assumed to be thermal (i.e., $v_{s_2} = 0$) and the HF beam is assigned a Mach number of 6. The distribution of relative energy is obtained from the relative velocity distribution by dividing the relative velocity distribution at each point by the relative velocity, i.e., $P(E) dE \propto [P(v_{rel})/v_{rel}] dv_{rel}$. Sample collision energy distributions are shown in Fig. 12. Note that the spread in collision energies increases markedly with increasing

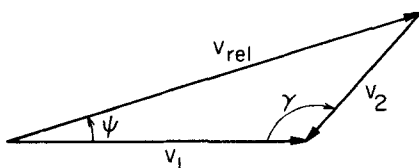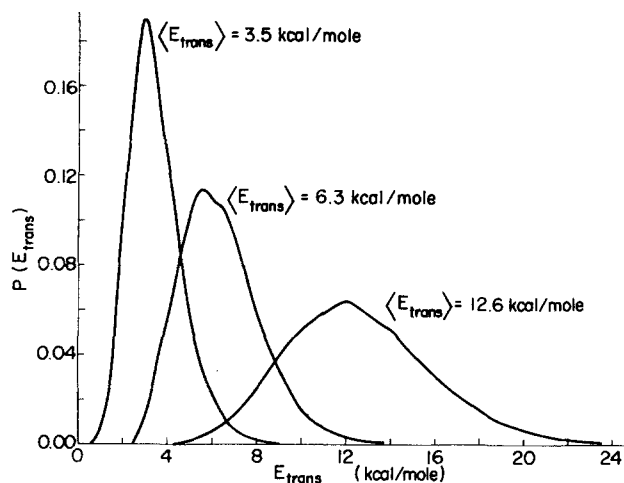FIG. 12. Calculated collision energy distributions for an assumed Mach number of 6. The total area has been normalized to unity.

collision energy. At high collision energies the spread is primarily due to the assumed value of the Mach number ($\mathfrak{M} = 6$).

[1] M. R. Levy, React. Kinet. Vol. 10(1–2), pp. 1–252 (1979).

[2] H. W. Cruse, P. J. Dagdigian, and R. N. Zare, Faraday Discuss. Chem. Soc. 55, 277 (1973).

[3] J. G. Pruett and R. N. Zare, J. Chem. Phys. 64, 1774 (1976). Note added in proof: A. Torres-Filho and J. G. Pruett, J. Chem. Phys. (to be published) have repeated the study of Ba + HF ($v = 1$). Contrary to earlier results, they find that low vibrational levels of BaF are populated predominantly by this reaction and that the reaction cross section for Ba + HF ($v = 1$) is approximately 3 times that for Ba + HF($v = 0$). Thus the effect of reagent vibration is similar to that of collision energy in regard to the reaction dynamics. A similar behavior is found for Sr + HF, as reported in Ref. 28. We are grateful to J. G. Pruett for communicating these results prior to publication.

[4] For example, see J. G. Pruett, F. R. Grabiner, and P. R. Brooks, J. Chem. Phys. 63, 1173 (1975); J. W. Hepburn, D. Klimek, K. Liu, J. C. Polanyi, and S. C. Wallace, ibid. 69, 431 (1978). See also Refs. 5 and 9 and references cited therein.

[5] K. T. Wu, H. F. Pang, and R. B. Bernstein, J. Chem. Phys. 68, 1064 (1978).

[6] L. Cowley, D. S. Horne, and J. C. Polanyi, Chem. Phys. Lett. 12, 144 (1971); A. M. G. Ding, L. J. Kirsch, D. S. Perry, J. C. Polanyi, and J. L. Schreiber, Faraday Discuss. Chem. Soc. 55, 252 (1973); J. C. Polanyi, J. T. Sloan, and J. Wanner, Chem. Phys. 13, 1 (1976); D. S. Perry and J. C. Polanyi, ibid. 12, 419 (1976).

[7] R. D. Coombe and G. C. Pimental, J. Chem. Phys. 59, 251 (1973).

[8] A. E. Redpath and M. Menzinger, Can. J. Chem. 49, 3063 (1971); D. M. Manos and J. M. Parson, J. Chem. Phys. 63, 3575 (1976).

[9] L. Pasternack and P. J. Dagdigian, J. Chem. Phys. 67, 3854 (1977).

[10] A. Siegel, Ph.D. thesis (Albert-Ludwigs Universität, Freiburg, Federal Republic of Germany, 1978); A. Siegel and A. Schultz, J. Chem. Phys. 72, 6225 (1980) (preceding paper).

[11] A. C. Luntz, IBM J. Res. Dev. 23, 956 (1979).

[12] Z. Karny and R. N. Zare, J. Chem. Phys. 68, 3360 (1978).

[13] For a discussion of nozzle beam expansions see J. B. Anderson in Molecular Beams and Low Density Gas Dynamics, edited by P. P. Wegener (Dekker, New York, 1974); H. Pauly

FIG. 11. Velocity diagram showing the relevant angles used in Eqs. (B2) and (B3).

and J. P. Toennies, *Methods of Experimental Physics*, edited by B. Bederson and W. L. Fite (Academic, New York, 1968), Vol. 7A.

[14] P. K. Sharma, E. L. Knuth, and W. S. Young, J. Chem. Phys. **64**, 4345 (1976).

[15] T. R. Dyke, B. J. Howard, and W. Klemperer [J. Chem. Phys. **56**, 2442 (1972)] reported that a substantial concentration of dimers may be formed on expansion of pure HF. Using a mass spectrometer, they measured the ratio of m/e of 21 (H_2F^+) to 20 (HF^+) and found that the ratio could be as high as 0.06. The parent ion of $(HF)_2$ is not observed and the ratio is likely to be only a lower bound to the fraction of dimers in the original beam. We have repeated these measurements under our conditions. For example, when 25 Torr of HF is expanded with 125 Torr of He at 300 °K, the mass ratio is 0.0005, while for 25 Torr of HF in 110 Torr of H_2 at 300 °K, the mass ratio is 0.004. However, we find that when similar experiments are carried out on HF in a D_2 carrier, mass peaks at 21 and 22 appear, indicating that part of the mass 21 peak observed with HF in H_2 originated from ion–molecule reactions in the ionization source.

[16] G. Herzberg, *Molecular Spectra and Molecular Structure I. Spectra of Diatomic Molecules* (Van Nostrand Reinhold, New York, 1950), pp. 257–264.

[17] In the BaF $C\,^2\Pi_{3/2}$–$X\,^2\Sigma^+$ subsystem, the band heads occur in the $R_2 + Q_{21}$ branches and in the R_{21} branch. For the (0,0) band, $J^{R_2+Q_{21}}_{head} \approx 75$ and $J^{R_{21}}_{head} \approx 228$. The latter would not be observed because it occurs at such a high J value and the R_{21} branch decreases in intensity with increasing J. The former does occur, but since the value of the $J^{R_2+Q_{21}}_{head}$ is about twice that of $J^{Q_1+R_{12}}_{head}$, the band heads in the BaF $C\,^2\Pi_{3/2}$–$X\,^2\Sigma^+$ subsystem are not so pronounced.

[18] See Z. Karny, R. C. Estler, and R. N. Zare, J. Chem. Phys. **69**, 5199 (1978). The original program has been corrected by W. H. Breckenridge and co-workers (University of Utah) and we are grateful to them for making a revised version of the program available to us. These corrections, however, do not affect the results of Karney *et al*.

[19] V. S. Kushawaha, Spectrosc. Lett. **6**, 633 (1973).

[20] R. D. Levine and R. B. Bernstein, Acc. Chem. Res. **7**, 393 (1974).

[21] Based on D_0^0(BaF) = 139.5 ± 1.6 kcal/mole from D. L. Hildenbrand, J. Chem. Phys. **48**, 3657 (1968).

[22] The Franck–Condon factors $q_{v',v''}$ used are $q_{0,0} = 0.9868$; $q_{1,1} = 0.9614$, $q_{2,2} = 0.9375$; $q_{3,3} = 0.9151$; $q_{4,4} = 0.8943$; $q_{5,5} = 0.8749$; $q_{6,6} = 0.8568$; $q_{7,7} = 0.8401$; $q_{8,8} = 0.8249$; $q_{9,9} = 0.8105$; $q_{10,10} = 0.7974$; $q_{11,11} = 0.7853$; $q_{12,12} = 0.7741$; $q_{13,13} = 0.7637$; $q_{14,14} = 0.7540$; $q_{15,15} = 0.7460$. Values for $q_{0,0}$–$q_{9,9}$ have been obtained from Ref. 2 and the others by extrapolation.

[23] L. T. Earls, Phys. Rev. **48**, 423 (1935).

[24] See R. D. Levine and R. B. Bernstein, *Molecular Reaction Dynamics* (Oxford U. P., New York, 1974), pp. 207–211. The contours in these equilateral triangle plots have the same significance as the contours in the right triangle plots of Polanyi and co-workers (see, for example, Ref. 6). Therefore the two types of triangle plots may be compared directly.

[25] T. M. Mayer, B. E. Wilcomb, and R. B. Bernstein, J. Chem. Phys. **67**, 3507 (1977).

[26] M. Menzinger and A. Yokozeki, Chem. Phys. **22**, 273 (1977).

[27] See Eqs. (8) and (9) of M. Menzinger and R. Wolfgang, Angew. Chem. Int. Ed. Engl. **8**, 438 (1969).

[28] A. Gupta, D. S. Perry, and R. N. Zare, J. Chem. Phys. **72**, 6248 (1980) (following paper).

[29] D. R. Herschbach, Discuss. Faraday Soc. **33**, 381 (1962).

[30] N. H. Hijazi and J. C. Polanyi, J. Chem. Phys. **63**, 2249 (1975); Chem. Phys. **11**, 1 (1975).

[31] P. Pechukas, J. C. Light, and C. Rankin, J. Chem. Phys. **44**, 794 (1968); J. Lin and J. Light, *ibid*. **45**, 2545 (1966); J. C. Light, Discuss. Faraday Soc. **44**, 14 (1968).

[32] D. G. Truhlar, J. Chem. Phys. **54**, 2635 (1971).

[33] P. J. Dagdigian, H. W. Cruse, A. Schultz, and R. N. Zare, J. Chem. Phys. **61**, 4450 (1974).

[34] The $C^{(6)}$ constants for the reactants and products are estimated as the sum of a Slater–Kirkwood dispersion term (induced dipole-induced dipole) and an induction term (dipole-induced dipole). The parameters used are: for the polarizability α(Ba) = 39.7 Å³, α(HF) = 0.506 Å³, α(BaF) = 18.5 Å³, and α(H) = 0.667 Å³; and for the dipole moment μ(HF) = 1.83 D and μ(BaF) = 8.0 D. The value of α(BaF) is estimated as the sum of α(Ba⁺) and α(F⁻); and the value of μ(BaF) is assumed to be about the same as μ(BaO).

[35] P. J. Kuntz, E. M. Nemeth, J. C. Polanyi, S. D. Rosner, and E. C. Young, J. Chem. Phys. **44**, 1168 (1966).

[36] H. Schorr, S. Chapman, S. Green, and R. N. Zare, J. Chem. Phys. **69**, 3790 (1978).

[37] L. Pasternack and P. J. Dagdigian, Rev. Sci. Instrum. **48**, 226 (1977).

[38] B. E. Wilcomb, J. A. Haberman, R. W. Bickes, T. M. Mayer, and R. B. Bernstein, J. Chem. Phys. **64**, 3501 (1976).

[39] W. S. Young, Rev. Sci. Instrum. **44**, 715 (1973).

[40] R. J. Gallagher and J. B. Fenn, J. Chem. Phys. **60**, 3492 (1974).

[41] J. B. Anderson and J. B. Fenn, Phys. Fluids **8**, 780 (1965).

[42] S. Datz, D. R. Herschbach, and E. H. Taylor, J. Chem. Phys. **35**, 1549 (1961).

[43] M. Cavallini, M. G. Dondi, G. Scoles, and V. Valbusa, Entropie **42**, 136 (1971).

[44] Equation (B6) is similar to Eq. (12) of Ref. 42. When one sets $v_{s1} = 0$, $v_{s2} = 0$, $\alpha_{s1} = \alpha_1$, $\alpha_{s2} = \alpha_2$, Eq. (B6) becomes essentially Eq. (12).